Environment-Aware Link Quality Prediction for Millimeter-Wave Wireless LANs

Yuchen Liu
Department of Computer Science,
North Carolina State University,
Raleigh, NC, USA
yuchen.liu@ncsu.edu

Douglas M. Blough
School of Electrical & Computer Engineering,
Georgia Institute of Technology,
Atlanta, GA, USA
doug.blough@ece.gatech.edu

ABSTRACT

Millimeter-wave (mmWave) communications have been regarded as one of the most promising solutions to deliver ultra-high data rates in wireless local-area networks. A significant barrier to delivering consistently high rate performance is the rapid variation in quality of mmWave links due to blockages and small changes in user locations. If link quality can be predicted in advance, proactive resource allocation techniques such as link-quality-aware scheduling can be used to mitigate this problem. In this paper, we propose a link quality prediction scheme based on knowledge of the environment. We use geometric analysis to identify the shadowed regions that separate LoS and NLoS scenarios, and build LoS and NLoS link-quality predictors based on an analytical model and a regression-based approach, respectively. For the more challenging NLoS case, we use a synthetic dataset generator with accurate ray tracing analysis to train a deep neural network (DNN) to learn the mapping between environment features and link quality. We then use the DNN to efficiently construct a map of link quality predictions within given environments. Extensive evaluations with additional synthetically generated scenarios show a very high prediction accuracy for our solution. We also experimentally verify the scheme by applying it to predict link quality in an actual 802.11ad environment, and the results show a close agreement between predicted values and measurements of link quality.

CCS CONCEPTS

• **Networks** → **Network performance modeling**; **Network performance analysis**; **Network experimentation**.

KEYWORDS

Millimeter wave; link quality; WLAN; prediction; machine learning.

ACM Reference Format:
Yuchen Liu and Douglas M. Blough. 2022. Environment-Aware Link Quality Prediction for Millimeter-Wave Wireless LANs. In *Proceedings of the 20th ACM International Symposium on Mobility Management and Wireless Access (MobiWac '22), October 24–28, 2022, Montreal, QC, Canada.* ACM, New York, NY, USA, 10 pages. https://doi.org/10.1145/3551660.3560912

MobiWac '22, October 24–28, 2022, Montreal, Canada

ACM ISBN 978-1-4503-9480-2/22/10.
https://doi.org/10.1145/3551660.3560912

1 INTRODUCTION

With the emergence of various bandwidth-intensive applications in recent years, e.g. virtual reality, online gaming, high-definition (HD) video streaming and holographic projection, wireless data traffic has been exponentially increasing, which places stricter requirements on throughput, reliability, and latency of wireless networks. In this regard, millimeter-wave (mmWave) communication is widely regarded as a key technology for future wireless networks, which can potentially achieve an order of magnitude higher data rate as compared to communication at sub-6 GHz frequencies. Several standardization efforts, such as IEEE 802.11ad/ay, are focused on 60 GHz mmWave communications for wireless local-area networks (WLANs) [1, 2] with a goal of achieving multi-Gbps data rates to satisfy bandwidth-hungry applications.

However, the shorter wavelengths at higher frequencies makes mmWave networks susceptible to link failures or rapid link quality decreases due to blockages in the environment. The susceptibility of links to blockage effects from obstacles such as walls and furniture items makes it difficult to predict link performance (e.g., signal-to-noise ratio) since small changes in the distribution of obstacles or the location of a client device can have a dramatic impact on the quality of a mmWave link. In mmWave WLANs, maintaining continuously high link quality is essential to meet the requirements of emerging applications, thus having the knowledge of link quality at locations of interest will significantly enhance network management. To be specific, the quality of service experienced by mobile users may be able to be significantly enhanced if information about future link quality along the users' routes is used for proactive resource allocation [3, 4]. Typically, a high-quality mmWave link must use a line-of-sight (LoS) path between sender and receiver [5]. However, when objects made of highly reflective materials such as metal are present in the environment, reflected paths can be found to maintain high link quality even when no LoS path exists between the two endpoints. Thus, a major difference in link quality prediction for mmWave networks is that knowledge of the environment, e.g., the locations and reflective properties of obstacles, is essential to perform accurate prediction.

The fundamental difference between link quality in the mmWave bands compared to lower frequencies is the stark difference between LoS and non-LoS (NLoS) cases. The LoS path component is predominant over NLoS components even in the presence of obstacles, and therefore the link quality under these scenarios is typically high and mainly dependent on the separation distance between the transceiver. Therefore, the primary challenge is to predict link quality under NLoS conditions where, as mentioned earlier, the quality

is highly dependent on the locations of surrounding obstacles and their reflectivity properties.

In this work, we propose a link quality prediction scheme for mmWave WLANs that takes into account the environment characteristics. We first use a geometric method to separate the LoS and NLoS areas in a given network scenario based on knowledge of obstacles' sizes and locations. We then propose LoS and NLoS link-quality predictors based on an analytical model and a regression-based approach, respectively. To be specific, for the more challenging NLoS scenarios, we generate a large data set with obstacles of varying sizes, locations, and material properties in different scenarios. Then, a ray-tracing technique is used to estimate ground-truth data on link quality for different locations in each data set instance. Measurement studies have demonstrated that the signal profiles produced by ray-tracing techniques are quite close to real measurements in mmWave scenarios [6]. Based on this, we use these data to train an artificial neural network to predict link quality given an obstacle scenario and user location. The derived link quality predictor is then used to construct a map of link quality predictions within the intended mmWave access point (AP) coverage area. Note that our prediction approach addresses blockages due to static obstacles to permit link quality prediction several seconds into the future to facilitate proactive resource allocation. Existing techniques address short-term predictions due to environment dynamics such as body blockages [7, 8] but allow less time for optimizing resources to deal with link quality changes.

The main contributions of this work are as follows.

- We propose the design of a mmWave link quality prediction framework that includes predictors for both LoS and NLoS locations. This framework can be used to efficiently construct a complete map of link quality predictions within a given environment, which could provide a basis for the development of anticipatory network management with proactive resource-allocation schemes.
- We develop for the first time a method to synthetically generate high-quality training data covering a wide range of fine-grained WLAN scenarios, which is then used to develop a machine learning and regression-based approach to link quality prediction for the challenging NLoS case. This provides the first link quality prediction scheme that is capable of predicting quality at *arbitrary* locations, i.e. not only at locations that have been previously visited and measured.
- We perform both simulations and real-world experiments to evaluate our link quality prediction scheme, which shows very good agreement with both synthetic data and actual measurements. This demonstrates that mmWave link quality can be accurately predicted through the use of detailed environment information.

2 RELATED WORK

Recent studies mainly considered the problem of *blockage prediction* with the aim of predicting when blockages will occur, and to proactively initiate countermeasures [9]. For example, [10, 11] used sub-6 GHz channels to predict blockages in the mmWave bands, and [7, 12] adopted recurrent neural networks to learn the spatio-temporal correlation of blockages. Furthermore, [13–15] used the visual information from cameras or videos to increase the accuracy of such predictors, where the effective prediction interval is limited to the duration of these visual features. A limitation of these approaches is that blockages do not always cause a substantial drop in mmWave link performance as sometimes opportunistic NLoS paths can be found that maintain a high link quality, e.g. when highly reflective obstacles are present. By contrast, our work herein focuses on *link quality prediction* since that is what drives network management decisions, e.g., AP association/handover and resource allocation.

Link forecasting involves predicting the quality and/or specific parameters of the wireless channel at a given location. Conventional approaches, e.g. [16, 17], measure the channel state information (CSI) of neighbouring APs to estimate link quality, which is an appropriate technique for sub-6 GHz frequencies. However, CSI-based link quality prediction is not a suitable approach in mmWave networks since the instantaneous CSI is not always attainable and applicable to predict the link quality at new locations. Several prior works predict path loss using analytical methods, e.g. [18] uses information about height and location of nearby buildings to predict the shadowing component of path loss, while other works, e.g. [19, 20], use path loss measurements at certain locations to predict path loss at other locations for conventional cellular or ad hoc networks. The latter approaches, however, are not suitable for mmWave-specific networks especially under NLoS conditions. As link quality is strongly dependent on client location, some prior works have considered joint prediction of link quality and mobility, e.g. [21, 22].

Several papers have discussed mmWave-specific link quality prediction [8][23][24]. In [8], the authors use a long short term memory based method to predict link quality from measurements in past time steps but the predictions work only for the next time step. Longer-term predictions based on mobility patterns and fixed obstacles are considered in [23] using a measurement-based approach. This work is discussed in detail below. In [24], a data driven model was employed to parameterize the path loss for mmWave channels in a given environment. However, this work only predicts link quality from separation distance based on the estimated parameters and, therefore, it does not account for the specific obstacle environment at a given location as our prediction model does.

The primary challenge we consider herein is to predict link quality for mmWave networks under NLoS conditions, where the quality is highly dependent on the locations of surrounding obstacles and their reflectivity properties. The only existing work we are aware of that addresses this problem is [23]. As mentioned earlier, this work adopts a measurement-based approach where link quality measurements are taken as clients move around to different locations and then those measurements are used as predictions for future transmissions at the same locations. While even a very small change in the locations could cause a big difference on the quality of mmWave link, it is impractical to measure every location of a scenario beforehand, thus this approach suffers from not being able to predict link quality at unknown locations. Also, it requires a period of preparation time to collect current measurement data for future prediction. By contrast, our approach can predict link quality at *any* location by capturing the details of the environment such as locations of obstacles and their reflectivities as well as room/AP

configurations. This then enables a complete map of link quality predictions to be efficiently constructed within a given scenario.

3 SYSTEM OVERVIEW

In mmWave WLANs, the diffraction ability of mmWave signal is much weaker and less reliable due to its smaller wavelength, which means that deployed objects in the environment have a significant impact on link performance. While these objects are prone to become obstacles blocking high-rate LoS links between APs and users, they also can act as reflectors to create alternative path components that might be useful when LoS transmission is blocked.

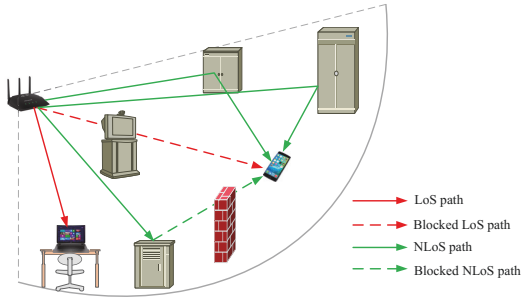

Figure 1: Path components in WLAN environments.

Motivating Example: Fig. 1 shows potential path components between an access point and user device, including blocked and unblocked LoS/NLoS paths. While the quality of a link under NLoS condition could drop substantially as compared to a LoS path, the AP can potentially avoid the blockage if there is a highly-reflective object nearby, which allows a high link quality to be maintained. However, reflection paths are also not reliable, because they may be blocked by other surrounding objects. Thus, the complex path distribution makes link quality extremely sensitive to node locations and environmental characteristics, e.g., room configuration, geometrical layouts and sizes as well as reflectivities of objects. The objective of this work is to construct an accurate mapping of the link quality at all locations within a given scenario based on knowledge of the deployed environment and without an extensive measurement campaign.

Technical Challenge: The major challenges in solving this problem are: 1) Due to the stark difference between link quality in LoS and NLoS cases in mmWave bands, the knowledge of the environment is essential to perform accurate prediction. However, it is analytically intractable to determine link quality from environment details; 2) Although machine learning techniques could be used to make link quality predictions, it is challenging to collect a sufficient volume of training data in real environment covering a complex range of WLAN scenarios. In particular, collecting large labeled datasets in the real world is prohibitively expensive and even impractical over a wide range of scenarios as it would require enormous human effort and complex infrastructure to accurately capture environment features and link quality; 3) Considering the potentially dramatic variation on link performance with even a small change in the location of a transmitter or receiver, there is no clear way to predict link quality at new locations that do not have prior measurements, especially being able to efficiently derive a complete map of link quality including locations that have not been previously visited.

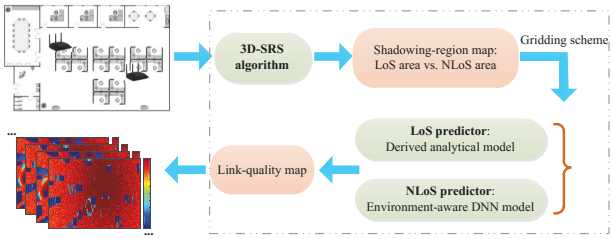

Figure 2: Architectural overview of environment-aware link quality prediction.

Solution Overview: Fig. 2 gives an overview of our environment-aware link quality prediction (ELP) framework that addresses the above challenges. First, a 3-dimensional shadowing-region search (SRS) approach is proposed to determine the LoS and NLoS areas of a given network scenario. Second, the region of the entire environment space is partitioned into groups of LoS and NLoS grid locations, which are then fed into the analytical model and trained deep neural network (DNN), respectively. In particular, we design a novel approach to generate high-quality network data for both training and evaluations. After obtaining the predicted link quality at each location, the complete set of link-quality maps are generated for deployed APs and all possible device heights. It is worth noting that the predicted link-quality maps pave the way to design *anticipatory networking* approaches for future wireless systems [25], e.g., performing proactive AP association/handover combining the link quality prediction with the user mobility information, and/or allowing the scheduler to adaptively schedule links when their quality is expected to be high. We will leave these promising directions as the future work, and in what follows, we discuss the details of technical components in our ELP framework.

4 LOS/NLOS AREA DETERMINATION

The fundamental difference between link quality in the mmWave bands compared to lower frequencies is the sharp difference between the LoS and NLoS cases. As a first step shown in Fig. 2, we use geometric analysis to identify the shadowed regions in an area that correspond to definite LoS/NLoS cases. Based on knowledge of the sizes and locations of obstacles (i.e., furniture items) in the indoor environment, we propose a 3D shadowing-region search (3D-SRS) approach to efficiently determine the LoS and NLoS areas in a given scenario, where a set of shadowing-region maps (see Fig. 3) are generated with respect to N_a APs and N_b height bases.

Algorithm 1 summarizes the steps of 3D-SRS algorithm. First, a floor plan of room S at each device height basis h_i is partitioned into N_g equal-sized grids with the gridding length of l_c, where $\bigcup_{i=1}^{N_g} g_i = S$ and $\bigcap_{i=1}^{N_g} g_i = \emptyset$. Considering all g_i in S at different device heights (Lines 1-5), the 2D grid set G and the shadowing-region (SR) map matrix Map are initialized. Next, the virtual heights of obstacles and AP are calculated with respect to different device height bases (Lines 7-8), and then we use the geometric analysis

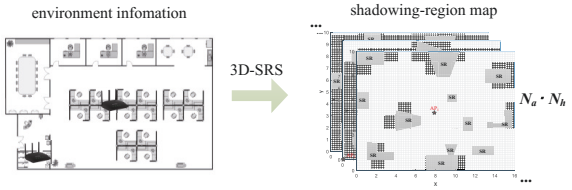

Figure 3: The schematic of LoS/NLoS areas determination.

to determine the shadowing-grid set SG_i given the information of obstacles and AP (Line 9). This geometric algorithm is based on a grid-based shadowing search (GSS) method [26], where the main idea is to check if the center point of a grid element exists in a shadowing polygon formed by an AP and known obstacles. To find all non-overlapped shadowed grids caused by different obstacles, the shadowed-grid set of each obstacle is first derived, and then the intersected grids over different shadowed-grid sets are eliminated. After traversing all known obstacles, the union of SG is obtained. Finally, we add these shadowed (i.e., NLoS) grids into *SR-Map* for each height basis h_i (Lines 10-13). The algorithm is terminated after all height bases are traversed.

Algorithm 1: 3D-SRS: 3D Shadowing-Region Search

Input: Obs, l_c, prm, N_g, H, ap
Output: *SR-Map*
1 **for** each height ($h_i = H_{min} + i * l_c$) & ($h_i <= H_{max}$) **do**
2 $G(i,:)$ = [all zeros in floor plan at height h_i];
3 ▽ init 3D map with all LoS grids
4 *SR-Map*$(i,:) = \vec{v}$(all zeros, size = N_g);
5 **end**
6 **for** each height h_i **do**
7 Obs.height = max{Obs.height - h_i, 0}; ▷ change the device height basis
8 ap.height = ap.height - h_i; ▷ get the virtual height of AP w.r.t device height basis
9 SG_i = FindSGset(Obs, ap, G, l_c); ▷ $\bigcup_{m \in obs} SG_{i,m}$
10 **for** each $j \in SG_i$ **do**
11 $k = SG_i(j)$;
12 *SR-Map*$(i, k) = 1$; ▷ NLoS grid location
13 **end**
14 **end**
15 **return** *SR-Map*;

5 LINK QUALITY PREDICTION

After determining LoS and NLoS scenarios, we present our link quality prediction scheme that separates LoS and NLoS cases. We first introduce an analytical method to estimate the link quality in LoS cases, and then propose a regression-based approach to predict link quality at NLoS locations by capturing the details of the environment.

5.1 LoS link-quality predictor

As we know, LoS path component contributes to the majority of link quality at mmWave frequencies (e.g., 60 GHz), which is predominant over NLoS components in the presence of obstacles. Therefore, the link performance under these scenarios is not highly dependent on surrounding obstacles, but instead, depends more on the distance between sender and receiver. Thus, we perform LoS link-quality predictions based on a 3GPP mmWave channel model with parameters chosen for indoor LoS scenarios [27]. To be specific, the path-loss model is derived as:

$$PL = 32.4 + 17.3 \cdot \log_{10}(d_{3D}) + 20 \cdot \log_{10}(f_c) + S_f, \quad (1)$$

where d_{3D} is the separation distance between the transceiver, f_c is the center frequency normalized by 1 GHz, and S_f is the shadowing factor that follows the normal distribution $\mathcal{N}(0, \sigma_{SF} = 3.0$ dB). In this way, signal-to-noise ratio ($\mathcal{S}$) can be further derived to quantify the link quality as:

$$\mathcal{S} = P_t \cdot G_t \cdot G_r \cdot (10^{PL/10} \cdot N_T)^{-1}, \quad (2)$$

where P_t is the transmit power, G_t and G_r are antenna gains at transmitter and receiver, respectively, PL is the path loss in Eq. (1), and N_T is the power of thermal noise. For any given LoS scenarios, we use this log-distance based LoS predictor to estimate the link quality in mmWave WLANs. We also evaluate the prediction performance of this analytical model with both simulations and actual measurements in Sec. 6-7.

5.2 NLoS link-quality predictor

When no LoS path exists, the quality of a mmWave is highly dependent on the node placements, locations of surrounding obstacles and their reflectivity properties. Treating these environmental parameters as independent variables and link quality as the dependent variable, a regression-based prediction approach naturally fits this situation. Accordingly, we develop and evaluate a machine learning and regression-based approach to prediction for these cases. Briefly, we first explore a framework to generate a large training data set with synthetically generated obstacles of varying sizes, locations, and material properties over a wide range of WLAN scenarios. Second, a mmWave ray tracer is used to produce ground-truth values of link quality at different locations of each scenario. Finally, we use this data to train a deep neural network (DNN) to predict link quality under NLoS scenarios.

1) Dataset generation framework

Here we introduce the fine-grained dataset generation (FDG) framework as shown in Fig. 4, which generates a large amount of high-quality training data across a wide range of WLAN scenarios.

Specifically, we first randomly generate various scenario cases with the following features: 1) the lengths, widths, and heights of rectangular room follow uniform distributions $L_r \sim \mathcal{U}(10.0, 20.0)$, $W_r \sim \mathcal{U}(5.0, 10.0)$, and $H_r \sim \mathcal{U}(2.4, 4.5)$; 2) Objects deployed in the room are modeled as cuboids and placed on the floor, where the center of each obstacle follows a Poisson point process with a specific density $\lambda \sim \mathcal{U}(0.04, 0.3)$, the widths, and lengths follow the truncated normal distributions W$\sim \mathcal{TN}(0.56, \sigma_w, 0.25, 1.25)$ and L$\sim \mathcal{TN}(1.08, \sigma_l, 0.5, 1.75)$, where $\sigma_w \sim \mathcal{U}(0.01, 0.38)$ and $\sigma_l \sim \mathcal{U}(0.08, 0.58)$. Their heights and orientations follow uniform distributions

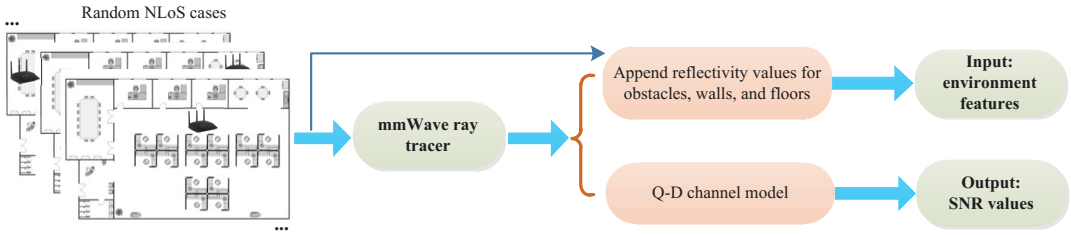

Figure 4: FDG framework overview.

$\Theta \sim \mathcal{U}(0, \pi)$ and $H \sim \mathcal{U}(0.3, 2.3)$); 3) each scenario case includes around 50 NLoS user locations, where each randomly-located client (i.e. wireless device) is viewed as a random point, and its height follows the uniform distribution $\mathcal{U}(0.1, 2.0)$. These parameters are derived by using a real-life office/lab environment as a guiding example, and all length units of parameters are in meters.

Second, we feed all generated scenario cases into our quasi-deterministic (Q-D) mmWave ray tracer [28], and do the following procedures. First, we assign the reflectivity values for obstacles, walls and floor in each scenario, where every obstacle material's reflection loss (dB) R_o follows the uniform distribution $\mathcal{U}(0.5, 30.0)$, the reflection loss (dB) of wall or floor is randomly chosen from the set {5.0, 15.0, 25.0}. The reflectivity parameters are derived based on the actual experiment measurements at 60 GHz from [29–31]. Next, these assigned reflectivity values are integrated with the environment information generated from the first step, thus all environment features of each scenario is obtained. In parallel, Q-D ray tracer is used to capture the geometrical properties of the channel for each transceiver and generate the profile of delay τ, path gain, angle of departure (AoD) θ_t, angle of arrival (AOA) θ_r, etc, for the path components in each NLoS case. Any small change in the location of a node translates into changes in these captured profiles.

Lastly, the output results from the ray tracer are directly used as input to a Q-D mmWave channel. Specifically, the Q-D mmWave channel can be characterized using a set of strong reflections and scattering rays, and the channel impulse response is defined as:

$$\begin{aligned} h(t) &= \sum_{\tau} \sum_{\theta_t} \sum_{\theta_r} Y_{tx}(\theta_t) \cdot Y_{rx}(\theta_r) \cdot h(t, \tau, \theta_t, \theta_r) \\ &= \sum_{i=0}^{N-1} 10^{-PL_i/20} e^{j\phi_i} \cdot (Y_{rx_i} \cdot Y_{tx_i}) \cdot e^{-j2\pi f \tau_i}, \end{aligned} \tag{3}$$

where N is the number of generated rays from ray tracer, PL_i (dB) and ϕ_i are the path loss and phase shift of ray i, and Y_{tx_i} and Y_{rx_i} are the radiation pattern of the transmitter and receiver array at ray i, respectively. To be specific, a power spectral representation of the 60 GHz signal is implemented, where the entire channel is divided into a number of equally spaced sub-bands, and each of them has the size of 5.156 MHz corresponding to the sub-carrier spacing for an orthogonal frequency division multiplexing (OFDM) PHY, while in single-carrier (SC) PHY mode, the power is divided equally across all the sub-bands over the entire bandwidth. With the input of the Q-D trace files from mmWave ray tracer, we parse these path profiles to obtain the spatial matrix between every transceiver pair. Specifically, the received power per sub-band Rx_i is computed and turned into a scalar value to represent the total energy apparent to the receiver by applying RF filtering as in [32], thus the overall received power is obtained by accumulating Rx_i over all sub-bands, and SNR value is further derived for each NLoS case.

Based on this FDG framework, we can effectively generate a large amount of training data including both detailed environment characteristics and SNR values, which is then used in a regression-based prediction model, discussed next.

2) SNR regression: a deep learning framework

We propose a DNN-based approach to predict NLoS link quality in mmWave WLAN, which takes into account the environment details as input features, and the problem to predict link quality for a NLoS scenario case is represented and solved in a supervised fashion.

a) Input feature and output label: We consider the availability of environment information including room configuration, obstacle sizes and locations, reflectivity information, the location of AP and client. The input data of DNN model is presented in the format of a concatenated vector V_e including all environment details. As shown in Eq. (4), for each sample case, the 3D Cartesian coordinates are used to indicate the client position $\mathcal{U}$, AP position $\mathcal{A}$, and room size $\mathcal{R}$. $\mathcal{N}_o$ represents the number of obstacles and $\mathcal{O}$ includes the locations, sizes, as well as reflectivities of obstacles. We use the zero-padding method to flatten the obstacle information $\mathcal{O}$ in different scenario cases. Note that the maximum number of generated obstacles N_m is equal to $(\lambda_m \cdot R_{l_m} \cdot R_{w_m})$, where λ_m, R_{l_m}, and R_{w_m} are the maximum obstacle density and room's length and width as defined in Sec. 5.2-1. By factoring in all environment details, the input feature vector $\mathcal{V}_e$ is obtained by concatenating above environment information with the size of $(6N_m + 12)$. On the other hand, the output label (ground truth) $\mathcal{S}_r$ used in DNN model is represented in the format of a SNR value. Finally, we post-process the input features and output values through a max-min normalization, which aims to eliminate the impact of scale differences among different features on the regression model.

$$\begin{aligned} \mathcal{V}_e = \{ &\mathcal{U}_{(x,y,z)}, \mathcal{A}_{(x,y,z)}, \mathcal{R}_{(x,y,z)}, \mathcal{N}_o, \mathcal{O}_{1(x,y,w,l,h,ref)}, ..., \\ &\mathcal{O}_{n-1(x,y,w,l,h,ref)}, \mathcal{O}_{n(x,y,w,l,h,ref)}, \mathcal{W}_{ref}, \mathcal{F}_{ref} \}. \end{aligned} \tag{4}$$

b) Network configuration: We use a deep neural network with the number of hidden layers and neurons configured to work across different network scenarios. The flattened input feature vector $\mathcal{V}_e$ of size n_{in} (N_m = 60) is fed to a fully connected network with 4 hidden layers as shown in Fig. 5. The l^{th} hidden layer has a total of n_k neurons. The k^{th} neuron in $(l-1)^{th}$ layer is connected to j^{th} neuron in l^{th} layer with a weight of w^l_{jk}. b^l_j represents the bias of

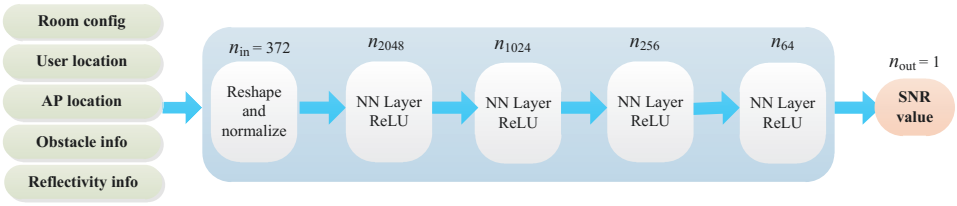

Figure 5: Model overview with data inputs (green), neural network model (blue), and output (red).

the j^{th} neuron in the l^{th} layer. The activation of the j^{th} neuron in the l^{th} layer, i.e. a_j^l, is calculated through the forward propagation rule as:

$$a_j^l = \max\{\sum_k w_{jk}^l a_k^{l-1} + b_j^l,\ 0\}, \tag{5}$$

Next, we use a sigmoid layer before the output layer to transform the output logits to normalized values. The model is trained through the backpropagation rule using a mean-squared error loss function. With the available training data bank, $DB = \{(\mathcal{V}_{e_1}, \mathcal{S}_{r_1}), (\mathcal{V}_{e_2}, \mathcal{S}_{r_2}), \ldots (\mathcal{V}_{e_N}, \mathcal{S}_{r_N})\}$, of N samples, the loss function is minimized using adaptive moment estimation optimization algorithm [33]. In particular, a batch of B training samples is randomly selected out of N training NLoS sample cases, and the weights w_j and biases b_j are updated through the following backpropagation rule:

$$\theta_{t+1} := \theta_t - \frac{\alpha \cdot m_t}{\sqrt{v_t} + \varepsilon} \tag{6}$$

$$m_t = \frac{\beta_1 m_{t-1} + (1-\beta_1) d\theta}{1 - {\beta_1}^t},\ v_t = \frac{\beta_2 v_{t-1} + (1-\beta_2) d\theta^2}{1 - {\beta_2}^t} \tag{7}$$

where a fraction of the gradient in the previous iteration t is retained with the coefficient of momentum, and the hyper-parameters β_1, β_2 and ϵ are set as 0.9, 0.999 and 10^{-8}, respectively. The learning rate α is initialized as 0.05 and decreased over time with decay factor of 0.9 for each 2,000 iterations, which aims to optimize prediction performance and increasing the convergence rate of the algorithm. In addition, the batch normalization technique is used to accelerate our deep network training with standardizing $\mathcal{V}_e$ to a layer for each batch, which dramatically reduces the number of training epochs required to train our predictor and also provides some regularization for reducing generalization error.

Note that the intuition behind this learning solution is that mmWave link quality is discoverable through the detailed environment information. Our properly-constructed network architecture with all tuned hyper-parameters is capable of learning from different scenarios and performing accurate prediction on link quality in unseen scenarios. We demonstrate this through detailed evaluations in Sec. 6.

In summary, based on the proposed link-quality predictors that separate LoS and NLoS scenarios, all predicted values at different locations and device heights can be eventually integrated into a combination of 2-dimensional link-quality maps as shown in Fig. 2. Note that, although the offline training process for the DNN model is time consuming due to the large amount of data needed to achieve good prediction accuracy, the online prediction process is fairly fast for both the analytical LoS model and trained NLoS regression model, thereby making our ELP solution less time-demanding. We report on link-quality map construction time in the next section.

6 EVALUATION RESULTS

In this section, we evaluate the performance of our approach to predict link quality in mmWave WLANs, which includes predictions for both LoS and NLoS scenarios.

6.1 Performance of LoS link quality predictor

First, we evaluate the performance of our analytical LoS prediction model. We generate various LoS cases and obtain the ground-truth SNR values by using the mmWave ray tracer and Q-D channel realization. Then, we use the approach derived in Sec. 5.1 to estimate the link quality for each LoS case, and the results are reported in Fig. 6.

Fig. 6 shows the comparison between the predicted SNR and ground truth at different user locations. As expected, we observe that link quality values are fairly high under LoS conditions, falling within a narrow range of 40–50 dB. On the other hand, it is noted that the gap between the predicted results and ground truths is quite small – the average SNR results are 45.54 dB and 46.12 dB, respectively (power of thermal noise is 7.04×10^{-12} Watts). This result demonstrates the feasibility of the log-distance based model to estimate link quality in LoS scenarios of mmWave WLAN, because the LoS path dominates the link quality at mmWave frequencies, which makes it mainly dependent on the separation distance between the sender and receiver rather than on the surrounding obstacles.

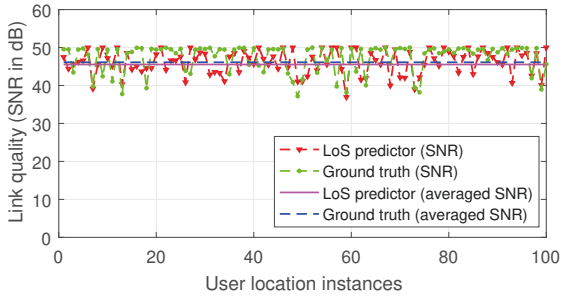

Figure 6: Link quality prediction comparison for LoS cases.

6.2 Performance of NLoS link quality predictor

Here, we evaluate our link quality prediction approach for the challenging NLoS cases, which are highly dependent on environment characteristics. We spent several months generating 600,000 data samples using our dataset generator (see Sec. 5.2-1)[1], split the data

[1]Note that this data generation time is not a serious issue, because it only has to be done once to generate the model and then it can be used as many times as needed for different room and obstacle environments.

into two sets, and conducted cross validation, where the training set was comprised of 90% of the data to learn the neural network parameters, and the remaining 10% of the dataset was used for validation and testing. We used TensorFlow and an NVIDIA P100 GPU to implement our DNN-based regression model, which was then used to predict the link quality in new instances, and we calculated the performance difference ratio (PDR) to measure the difference between the predicted values and ground truths. The PDR is defined as $|\mathcal{S}_{pred} - \mathcal{S}_{truth}|/(\mathcal{S}_{\max} - \mathcal{S}_{\min})$, where the denominator represents the difference between the maximum SNR and minimum SNR observed across all test data samples.

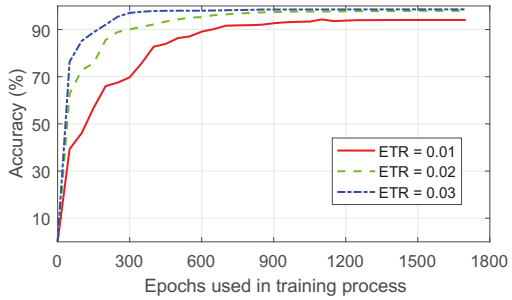

Figure 7: Prediction accuracy vs. number of training epochs.

First, we evaluate the prediction accuracy with varying *error tolerance rate* (ETR), where the predicted link quality $\mathcal{S}_{pred}$ is accepted as an accurate result when the PDR is less than the given ETR. Fig. 7 shows the prediction accuracy vs. the number of training epochs for different ETRs. As expected, the accuracy becomes higher as the number of epochs used to train the DNN model increases, where the prediction accuracy can achieve 93.86%, 97.89% and 98.54% for different ETRs with a sufficiently large number of epochs. On the other hand, a larger ETR provides a higher prediction accuracy and converges faster, which indicates that most predicted values can efficiently approximate the ground truth during the regression process.

To show finer-grained results, we evaluated the prediction accuracy vs. ETR, where the neural networks were trained until the accuracy performance of the test set did not improve for 300 epochs. We also show how many epochs were needed to reach the given accuracy. We note that a prediction accuracy of around 94% is achieved for an ETR of 0.01, which means that 94% of predicted values have a PDR of less than 0.01 as compared to the ground truth, which corresponds to a SNR difference of only 0.5 dB. In addition, almost 99% of predicted values can achieve a PDR of 0.035, which means the prediction is within 1.75 dB of the ground truth value.

Second, we evaluate the performance of our predictor for discrete instances within a mmWave WLAN. Here, we also report results for the log-distance based (LD) model from 3GPP Release 16 [27] as a comparison point. Fig. 9 shows the link quality results at different user locations. As compared to the results of LoS cases in Fig. 6, we observe that link quality fluctuates within a wider range due to its high environment dependency. When we examine the results of 3GPP LD model, the estimated link quality typically falls within a relatively narrower range of 15–35 dB, and over 70% of data instances underestimate the link quality in evaluated cases.

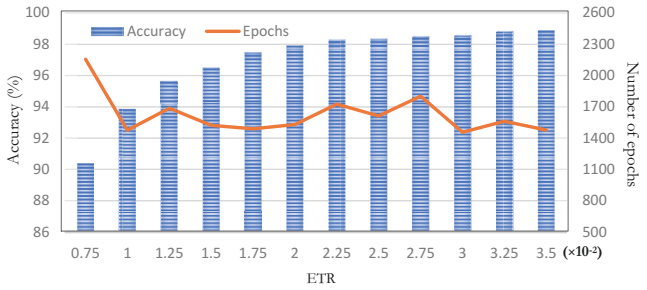

Figure 8: Prediction accuracy vs. ETR.

However, the predicted link quality from our predictor matches the ground-truth data well since it accounts for the environment characteristics.

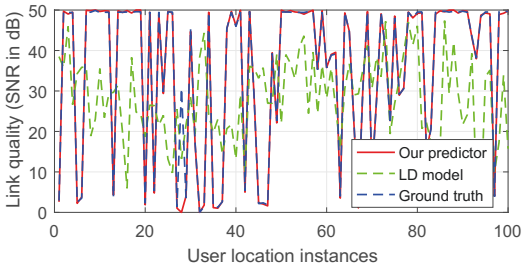

Figure 9: Link quality prediction comparison.

Lastly, we investigate the relative importance of different environment features on link quality prediction. Here we estimate the feature importance by using a weight-based analysis method [34], where the percentage of hidden nodes' weights attributable to a particular input node are computed to measure the importance of that input feature.

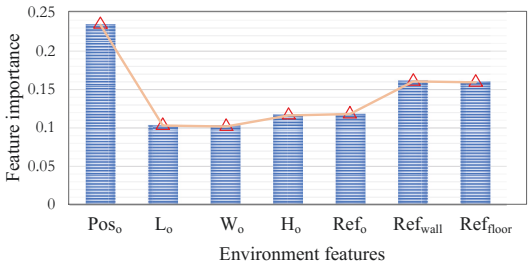

Figure 10: Importance of different environment features to NLoS link quality.

Fig. 10 shows the feature importance vs. different environment features, and we conclude several key insights on which features have more impact on the link quality variation under NLoS conditions: 1) The position of the obstacle is the most impactful factor for NLoS link quality, because a small change in any obstacle's location could easily block or create the potential path components that impact overall link quality. 2) Considering the obstacle's dimensions, the height has more impact than the length and width. This is reasonable since APs are deployed on the ceiling so that taller obstacles are closer to the AP, which could more easily impact the distribution of NLoS components. 3) Comparing the reflectivity

of obstacle, wall and floor, we observe that the reflectivity of wall and floor are more impactful, and this is because most stronger NLoS paths, e.g., the first-order reflection path, usually bounce off the wall or floor, as validated in [35], which makes their material reflectivities more critical in determining the overall link quality performance.

6.3 Link-quality map construction

In this part, we evaluate the performance of our end-to-end framework (see Fig. 2) to produce link-quality maps for a given network scenario. Fig. 11(a) shows a WLAN scenario with several obstacles and two APs deployed. We run our ELP framework to generate 2-dimensional link-quality maps for each AP and each possible device height. Fig. 11(b) and Fig. 11(c) show the two corresponding link-quality maps for a device height of 0.8m. With the maps of link quality, one can easily find the link quality at any location of a given scenario.

It is worth noting that, using our ELP framework, only 10.58 minutes are needed to generate the complete set of link-quality maps for two APs and all possible device heights (with gridding length of 0.1m) in the evaluated scenario.[2] In contrast, to generate one 2-D map, i.e. for one AP and one device height, a full ray-tracing calculation took more than two weeks. Therefore, constructing all maps using ray tracing is not practical since this would require more than 3 years of computation time for the given scenario.

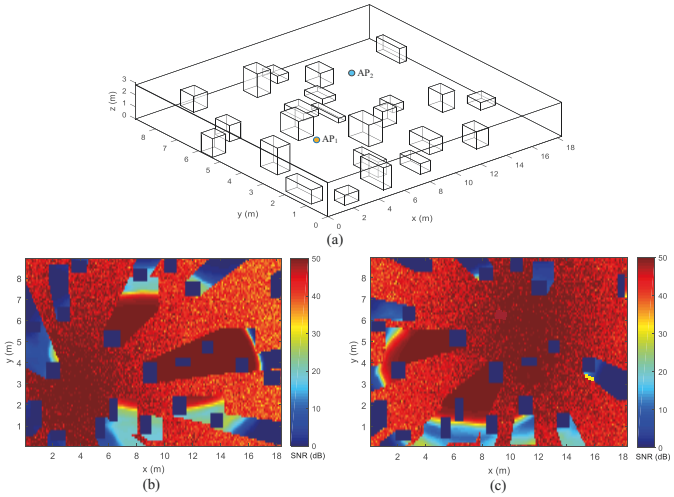

Figure 11: (a) Scenario example; (b)-(c) Link-quality maps for AP_1 and AP_2 (device height is 0.8m).

6.4 Discussion of required environment information

Our link quality predictor requires the input of some environment details, including locations, sizes, and material reflectivities of surrounding objects in a given scenario. In practice, objects' locations, sizes, and material types could be obtained in a variety of ways, e.g., through camera-based sensing, but it is non-trivial to get the exact reflectivity values of different objects. The reflectivity index can be estimated based on the knowledge of object material types from reported measurements, e.g. [29–31]. Because these values will not always match the actual reflectivities of objects in a given environment, in this subsection, we evaluate the robustness of our prediction framework to deviations of the reflectivity values.

Here, we add random noise to the reflectivity values of obstacles, walls, and the floor. The noise, which follows a normal distribution $\mathcal{N}\sim(0, var)$ in dB units, is added to the actual reflectivity loss chosen as described in Sec. 5.2. The disturbed reflectivity values combined with other required information are fed into our predictor while the undisturbed values are used for the ground truth calculation. We re-ran the accuracy evaluations from Sec. 6.2 to see how the variation of reflectivity values affects the link quality predictions.

Fig. 12 shows the prediction accuracy vs. different variances for the reflectivity noise values. Compared to the baseline with 0 dB variance, we observe that there is almost no impact on the accuracy performance with 1 dB of noise variance. When increasing *var* to 3 dB and 5 dB, the accuracy performance only degrades 1.6%–3% for ETR of 0.01 and 0.5%–2.5% for ETR of 0.03, respectively, which validates the robustness of our prediction method to the reflectivity inaccuracies. Thus we conclude that our proposed approach can tolerate reasonable deviations on the estimated reflectivity values, and maintain a good prediction accuracy without the need for exact reflectivity information.

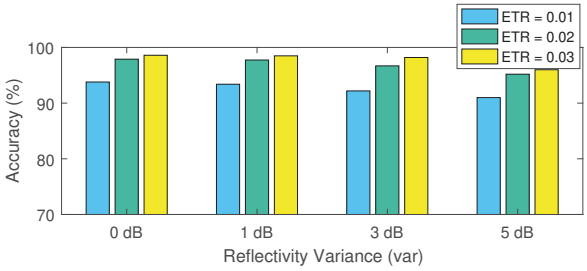

Figure 12: Prediction accuracy vs. reflectivity variance.

6.5 Discussion of impact of dynamic obstacles

Our proposed prediction approach deals with blockages due to static obstacles, which aims to permit link quality prediction several seconds into the future in a relatively stable environment. To investigate the feasibility of our predictor in scenarios with low-density dynamic obstacles (i.e., humans), here we conduct an evaluation with randomly moving humans inside of a room to see how they affect prediction accuracy. To be specific, we adopt the obstacle and mobility models of humans from [36], and then evaluate 5 different scenarios with a total of 500 locations. In each case, we evaluate the link quality variation due to moving obstacles at specific time instances, where the variation is quantified as the percentage difference between our predicted link quality and the ground-truth link quality with the human obstacles.

Fig. 13 shows the histogram of link quality variation under low human obstacle densities λ_h (/m^2). We observe that the gap between our link quality prediction and ground truth remains unchanged or varies within 2% (i.e., variation interval is [0, 2%]) for 80%-95% of both LoS and NLoS cases when λ_h is less than 0.1 (i.e., less than 10

[2]The running time is evaluated on an Intel(R) Core(TM) i5-6200U 2.3GHz CPU workstation with 2 cores and 4 logical processors.

humans in the 12m×8m room). This result validates the potential use of our prediction method in common office/lab scenarios with a relatively low density of dynamic obstacles.

To handle real-time link quality prediction in environments with a higher density of moving obstacles, our prediction approach could be augmented with dynamic prediction techniques, e.g. [7, 8] that address short-term predictions due to environment dynamics such as body blockages. To be more specific, based on our predicted link-quality map (e.g., Fig. 11), short-term prediction could be used to dynamically "cool down" "hot" areas (ones with higher link qualities) where dynamic obstacles are present, whereas in lower link-quality areas, the predictions would remain unchanged since moving obstacles will not help improve the link quality that has already been deteriorated by static obstacles. We leave a detailed evaluation of this augmented prediction approach as future work.

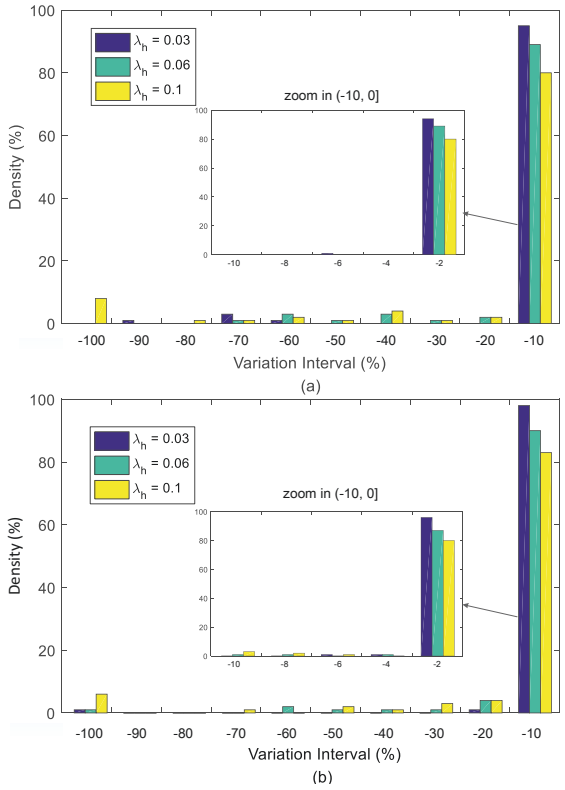

Figure 13: Distribution of variation in predicted and ground-truth link qualities during human obstacles in (a) LoS cases and (b) NLoS cases.

7 EXPERIMENTAL VALIDATION

To further validate the performance of our link quality prediction, we performed real-world measurements of link quality in an actual network environment and compared them to the predicted values.

Fig. 14(a) and (b) give an overview of the laboratory setup. Specifically, we conducted the experimental measurements in a 10m×6m×3m laboratory environment, and a TP-link Talon ad7200 router [37] mounted on the ceiling was used as the AP. The Talon router contains the Qualcomm QCA9500 chipset, which implements the IEEE 802.11ad standard. Then, we used an Acer Travelmate P648 laptop [38] as a client device to communicate with the AP. We measured the PHY-layer link quality (SNR) at different locations using the Linux `iperf3` and `iwconfig` tools. The entire laboratory scenario was precisely modeled with a number of cuboid-based obstacles as shown in Fig. 14(c), and we extracted the required environment features as the inputs to our link-quality predictor, which then generated the predicted values. We considered 20 user locations that consisted of 5 LoS cases and 15 NLoS cases. The performance comparisons between the prediction and measurement are reported in Fig. 15 and Fig. 16.

Fig. 15 shows the results of LoS scenarios, and it is observed that the predicted values are very close to the actual measurements at different LoS locations, with differences of only around 0.5–2 dB. This result is not surprising since the link quality is consistently high when there is a LoS path between the AP and the client.

For the NLoS cases in Fig. 16, we observe that the link quality is typically different at each location due to the changes in surrounding obstacles, but our predicted results can still achieve a good agreement with the measurement data. For instance, at locations #1, #5 and #12, high link quality is predicted since the client is located near a metal cabinet in the scenario. While extremely low link quality is predicted and observed at locations #2, #8 and #9 due to the long distance and lack of highly reflective objects nearby. Here the predicted values fairly consistently overestimate the link quality by about 3–5 dB, and we think this is due to the lack of a precise transmission power given in the specifications of the Talon AP used in the measurement. For prediction purposes, we chose a middle value within the specified transmission power range to train our predictor. However, with a calibration of around 4 dB, the differences can be reduced to achieve very close agreement with the actual measurement results.

8 CONCLUSION

In this paper, we studied link quality prediction in mmWave WLANs. By capturing the details of the environment such as locations of obstacles and their reflectivities, we separate the LoS and NLoS scenarios and propose an environment-aware prediction approach to predict link quality at any location of the scenario. In particular, a DNN-based regression model was trained to predict the link quality in difficult NLoS cases by using our synthetically generated data set. Both simulations and experiment measurements were performed to show that our approach can achieve high prediction accuracy and the predicted values are in close agreement with the actual measurements.

ACKNOWLEDGMENTS

This research was supported in part by the National Science Foundation through Awards CNS–1813242 and CNS–2016381.

REFERENCES

[1] IEEE Standard 802.11ad-2012. https://ieeexplore.ieee.org/stamp/stamp.jsp?arnumber=6392842
[2] IEEE Standard 802.11ay/Draft 7.0: *Wireless LAN Medium Access Control (MAC) and Physical Layer (PHY) Specifications— Amendment 2: Enhanced Throughput for Operation in License—Exempt Bands Above 45 GHz*, Dec. 2020.
[3] F. Firyaguna, A. Bonfante, J. Kibiłda, and N. Marchetti, "Performance evaluation of scheduling in 5G-mmWave networks under human blockage", *arXiv preprint arXiv:2007.13112*, 2020.

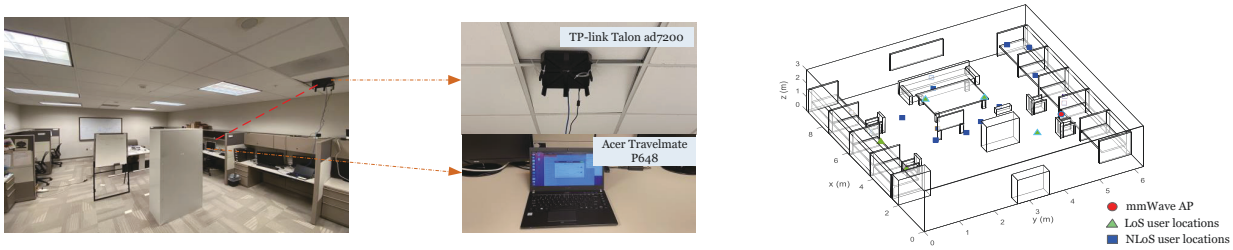

(a) (b) (c)

Figure 14: (a) Network scenario; (b) 802.11ad AP and client laptop; (c) Modeled scenario and measured user locations.

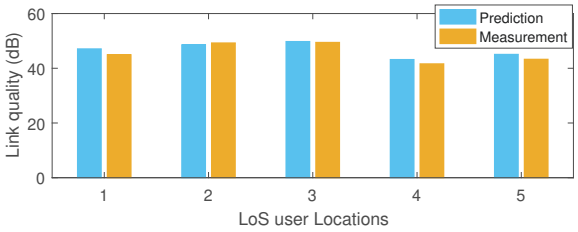

Figure 15: Link quality validation of LoS locations.

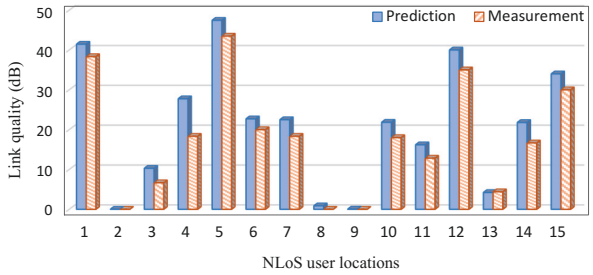

Figure 16: Link quality validation of NLoS locations.

[4] L. Shen, T. Wang, and S. Wang, "Proactive proportional fair: A novel scheduling algorithm based on future channel information in OFDMA systems", *Proc. of IEEE/CIC Int'l Conf. on Communications in China*, 2019.

[5] Y. Liu, Q. Hu, and D. Blough,"Joint link-level and network-level reconfiguration for mmWave backhaul survivability in urban environments", *Proc. of Int'l ACM Conference on Modeling, Analysis & Simulation of Wireless & Mobile Systems*, 2019.

[6] B. Neekzad, K. Sayrafian-Pour, J. Perez, and J. S. Baras, "Comparison of ray tracing simulations and millimeter wave channel sounding measurements", *Proc. of IEEE Int'l Symposium on Personal, Indoor, and Mobile Radio Communications*, 2007.

[7] A. Alkhateeb, I. Beltagy, and S. Alex, "Machine learning for reliable mmwave systems: Blockage prediction and proactive handoff", *Proc. of IEEE Global Signal Inf. Process*, 2018.

[8] S. Shah, M. Sharma, and S. Rangan, "LSTM-based multi-link prediction for mmwave and sub-THz wireless systems", *Proc. of IEEE Conf. on Commu.*, 2020.

[9] A. Kalor, O. Simeone, and P. Popovski, "Latency-constrained prediction of mmWave/THz link blockages through meta-learning", arXiv preprint arXiv:2106.07442, 2021.

[10] Z. Ali, A. Duel-Hallen, and H. Hallen, "Early warning of mmWave signal blockage and AOA transition using sub-6 GHz observations", *IEEE Commun. Letters*, 2019.

[11] D. Burghal, R. Wang, and A. Molisch, "Deep learning and Gaussian process based band assignment in dual band systems," arXiv preprint:1902.10890, 2019.

[12] M. Hussain, M. Scalabrin, M. Rossi, and N. Michelusi, "Mobility and blockage-aware communications in millimeter-wave vehicular networks", *IEEE Transaction on Vehicular Technology*, 2020.

[13] G. Charan, M. Alrabeiah, and A. Alkhateeb, "Vision-aided 6G wireless communications: Blockage prediction and proactive handoff", arXiv preprint arXiv:2102.09527, 2021.

[14] M. Alrabeiah, A. Hredzak, and A. Alkhateeb, "Millimeter wave base stations with cameras: Vision-aided beam and blockage prediction", *Proc. of IEEE VTC*, 2020.

[15] Y. Koda, K. Nakashima, K. Yamamoto, T. Nishio, and M. Morikura, "Handover management for mmWave networks with proactive performance prediction using camera images and deep reinforcement learning", *IEEE Trans. on Cognitive Commu. and Netw.*, 2019, 6(2), 802–816.

[16] J. Joo, M. Park, D. Han, and V. Pejovic, "Deep learning-based channel prediction in realistic vehicular communications", *IEEE Access*, 2019.

[17] C. Luo, J. Ji, Q. Wang, X. Chen, and P. Li, "Channel state information prediction for 5G wireless communications: A deep learning approach", *IEEE Transactions on Network Science and Engineering*, 2018.

[18] M. Piacentini and F. Rinaldi,"Path loss prediction in urban environment using learning machines and dimensionality reduction techniques", *Computational Management Science*, 2014, 8(1), 371–384.

[19] M. Kasparick, R. Cavalcante, S. Valentin, S. Stanczak, and M. Yukawa, "Kernel-based adaptive online reconstruction of coverage maps with side information", *IEEE Transactions on Vehicular Technology*, 2015.

[20] E. DallAnese, S. Kim, and G. Giannakis, "Channel gain map tracking via distributed kriging", *IEEE Trans. on Vehicular Technology*, 2011.

[21] L. Muppirisetty, T. Svensson, and H. Wymeersch, "Spatial wireless channel prediction under location uncertainty", *IEEE Trans. on Wireless Commun.*, 2016.

[22] N. Bui and J. Widmer, "Mobile network resource optimization under imperfect prediction", *IEEE World of Wireless, Mobile and Multimedia Networks*, 2015.

[23] J. Palacios, P. Casari, H. Assasa, and J Widmer, "LEAP: Location estimation and predictive handover with consumer-grade mmWave devices", *Proc. of IEEE Int'l. Conference on Computer Communications*, 2019.

[24] M. Neema and E. S. Gopi, "Data driven approach for mmWave channel characteristics prediction using deep neural network", *Wireless Personal Communications*, 2021, 120.3, 2161-2177.

[25] N. Bui, M. Cesana, S. Hosseini, Q. Liao, I. Malanchini, and J. Widmer, "A survey of anticipatory mobile networking: Context-based classification, prediction methodologies, and optimization techniques", *IEEE Communications Surveys & Tutorials*, 2017, 19(3), 1790–1821.

[26] Y. Liu, Y. Jian, et al., "Maximizing line-of-sight coverage for mmWave wireless LANs with multiple access points", *IEEE/ACM Transactions on Networking*, 2021.

[27] 3GPP TR, "Study on channel model for frequencies from 0.5 to 100 GHz", 2019.

[28] "MmWave ray tracer for WLAN data generation", https://github.com/yuchen-sh/mmWave_ray_tracer.

[29] J. Lu, D. Steinbach, P. Cabrol, P. Pietraski, and R. Pragada, "Propagation characterization of an office building in the 60 GHz band", *Proc. of IEEE European Conference on Antennas and Propagation*, 2014.

[30] K. Sato, T. Manabe, T. Ihara, et al. "Measurements of reflection and transmission characteristics of interior structures of office building in the 60-GHz band", *IEEE Transactions on Antennas and Propagation*, 1997, 45(12), 1783-1792.

[31] M. Samimi, and T. Rappaport, "Characterization of the 28 GHz millimeter-wave dense urban channel for future 5G mobile cellular", *NYU Wireless TR* 1, 2014.

[32] H. Assasa, J. Widmer, et al., "Enhancing the ns-3 IEEE 802.11 ad model fidelity: Beam codebooks, multi-antenna beamforming training, and quasi-deterministic mmWave channel", *Proc. of ACM Workshop on ns-3*, 2019.

[33] D. Kingma and J. Ba, "Adam: A method for stochastic optimization", 2014, arXiv preprint arXiv:1412.6980.

[34] J. Heaton, S. McElwee, J. Fraley, and J. Cannady, "Early stabilizing feature importance for TensorFlow deep neural networks", *Proc. of IEEE International Joint Conference on Neural Networks*, 2017.

[35] A. Deng, Y. Liu and D. Blough, "Maximizing coverage for mmWave WLANs with dedicated reflectors", *Proc. of IEEE Int'l Conference on Communications*, 2021.

[36] Y. Liu, and D. Blough, "Blockage robustness in access point association for mmWave wireless LANs with mobility", *Proc. of Local Computer Networks*, 2020.

[37] TP-Link Talon AD7200 Wi-Fi Router, URL: https://www.pcmag.com/review/347405/tp-link-talon-ad7200-multi-band-wi-fi-router

[38] Acer TravelMate P648, URL: https://www.acer.com/ac/en/US/press/2016/175243